

Optimized ZT of Bi_2Te_3 - GeTe compounds from first principles guided by homogeneous dataJae Nyeong Kim,¹ Massoud Kaviani,^{2,3} and Ji-Hoon Shim^{1,3,4,*}¹*Department of Chemistry, Pohang University of Science and Technology, Pohang 37673, Korea*²*Department of Mechanical Engineering, University of Michigan, Ann Arbor, Michigan 48109-2125, USA*³*Division of Advanced Nuclear Engineering, Pohang University of Science and Technology, Pohang 37673, Korea*⁴*Department of Physics, Pohang University of Science and Technology, Pohang 37673, Korea*

(Received 5 January 2016; published 9 February 2016)

We predict the thermoelectric properties of layered $[\text{GeTe}]_m[\text{Bi}_2\text{Te}_3]_n$ (GBT) compounds ($1 \leq m \leq 8, 1 \leq n \leq 3$), using first-principles-Boltzmann transport calculations of the homogeneous (Bi_2Te_3 and GeTe) data. The lattice strain and the quantum-confinement effects of compounds evolve the band-gap structures, resulting in asymmetric and large Seebeck coefficient, at high GeTe content. Using semiempirical calculations of electron scattering rate $1/\tau_e$, dominated by electron-acoustic phonon scattering, we reproduce reported TE properties of GBT compounds. We predict that, due to small Seebeck coefficient, the GBT compounds with high n - and p -type doping ($\sim 10^{20} \text{ cm}^{-3}$), do not have high ZT near room temperature. However, we predict that the moderately doped ($\sim 10^{19} \text{ cm}^{-3}$), p -type GBT compounds have enhanced $ZT \approx 1.4$ near room temperature.

DOI: 10.1103/PhysRevB.93.075119

I. INTRODUCTION

The layer mixing of a heterostructure is promising for enhancing thermoelectric (TE) properties, i.e., the figure of merit $ZT = S^2\sigma T/\rho\kappa$, where S is the Seebeck coefficient, σ is the electrical conductivity, κ is the thermal conductivity, and T is the absolute temperature [1–9]. Intrinsic interface effect modifies the electrical properties by altering the band structures and the band-gap energy. Also the phonon scattering at the interface reduces the lattice thermal conductivity (κ_l), which can dominate κ .

The $[\text{GeTe}]_m[\text{Bi}_2\text{Te}_3]_n$ (GBT) compounds, Fig. 1, are naturally mixed-layer compounds of two distinct TE materials, GeTe and Bi_2Te_3 [10–15], having the same rhombohedral symmetry (space group $R3m$, 160). So, GBT compounds with (m,n) can be synthesized, and these as well as the $\text{GeTe-Sb}_2\text{Te}_3$ (GST) compounds have also been used in phase-change memory devices due to their amorphous to cubic/rhombohedral crystal phase transition upon thermal annealing [16–18]. There have been studies on their TE properties with ZT of 0.2–0.5 at room temperature [12–15,19]. Recently, $[\text{GeTe}]_{0.95}[\text{Bi}_2\text{Te}_3]_{0.05}$ and $[\text{Ge}_{0.87}\text{Pb}_{0.13}\text{Te}]_{0.97}[\text{Bi}_2\text{Te}_3]_{0.03}$ have been reported with high ZT of 1.6 and 2.0, respectively, so the mixture of the two compounds could also be considered promising [20,21]. The GBT nanowires were synthesized at various compositions, showing that reduced dimensionality and electrical anisotropy enhance TE properties [22]. Theoretically, $\text{PbTe-Bi}_2\text{Te}_3$ (PBT) compounds have been predicted to have larger band-gap energy than Bi_2Te_3 and improved TE properties with intermediate operating temperatures [23]. Other theoretical studies of these compounds have been focused on their topological properties [24–27].

Here we investigate the electronic structures and TE properties of GBT compounds, using density functional theory (DFT) [28,29] and the Boltzmann transport equations (BTEs) [30]. We explore GBT compositions ($1 \leq m \leq 8$,

$1 \leq n \leq 3$) over a range of temperature 100–500 K. There have been few studies with controlled carrier concentration in GBT compounds [12,19], so we consider two representative carrier concentrations: 10^{19} cm^{-3} and $4 \times 10^{20} \text{ cm}^{-3}$. By employing a semiempirical presentation of electron scattering time (τ_e), we first successfully reproduce the reported ZT of Bi_2Te_3 and several GBT compounds. Then we proceed to other compounds and predict that their room temperature ZT can reach up to 1.4 for $m = 8$ and $n = 1$.

II. METHODS

We used the Vienna *ab initio* simulation package (VASP) code for finding optimal crystal structure (both lattice constants and atomic positions) of homogeneous GBT compounds in the range of $1 \leq m \leq 8$ and $1 \leq n \leq 3$ [28]. In the DFT calculation, the projector augmented wave (PAW) method was used with the generalized gradient approximation by Perdew, Burke, and Ernzerhof (PBE GGA) as an exchange correlation potential [31]. The cutoff energy in the plane-wave expansion of the valence states was set to 500 eV, and the self-consistent-field convergence thresholds were 10^{-4} eV and 0.001 eV/Å for the total electronic energy and force, respectively. The Γ -centered $8 \times 8 \times 2k$ mesh was used in the full Brillouin zone (BZ). To treat heavy Bi atoms, we have considered the spin-orbit (SO) coupling. To consider van der Waals (vdW) interaction, we also have considered the Grimme method (DFT-D2) [32]. For empirical C_6 and R_0 parameters of Ge and Te, we followed those reported [32] and used $C_6 = 63.55 \text{ J nm}^6/\text{mol}$ and $R_0 = 1.9 \text{ \AA}$ for Bi [33].

Based on the relaxed crystal structures, we calculate the electronic structure of GBT compounds by using the WIEN2K code [29], which uses a full potential linearized augmented plane wave+local orbitals (L/APW+LO) methods based on the DFT. For the estimation of the band gap, we have tested both PBE GGA and EV GGA (GGA by Engel and Vosko) [34] for the exchange correlation potential and found that two results give similar trends, so we only show the results using the PBE GGA. As the nonoverlapping radius of muffin tin (RMT), 2.5 in atomic units was used for all atomic

*Corresponding author: jhshim@postech.ac.kr

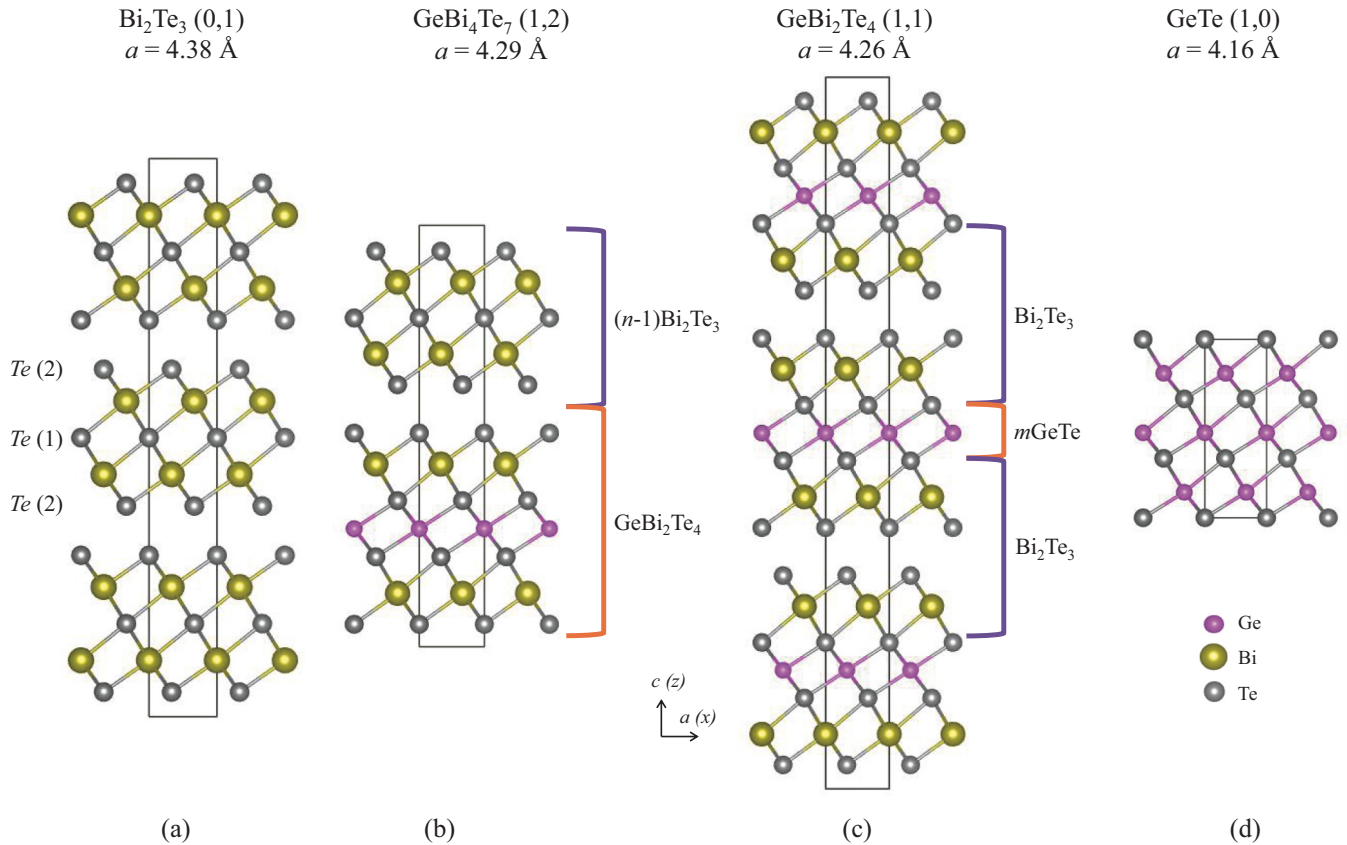


FIG. 1. Side view of crystal structures for GBT compounds with (m, n) compositions of GeTe and Bi_2Te_3 , guided by the lattice constant a . The colors identify Ge (purple), Bi (yellow), and Te (gray) atoms. The crystal structures are obtained by the VESTA program [72].

species. The $10 \times 10 \times 10k$ mesh is used for the self-consistent charge density calculation and dense $36 \times 36 \times 36k$ mesh is used for precise description of the TE properties. Using the calculated electronic structures and rigid band approach, the TE properties are calculated with semiclassical BTE implemented in the BOLTZTRAP code [30]. In the BTE, we consider the temperature-dependent τ_e with semiempirical treatment which will be described in Sec. III C.

III. RESULTS AND DISCUSSION

A. Crystal and electronic structures

The crystal structures of homogeneous GBT compounds are summarized in Fig. 1 [10,11,15]. According to the reports by Kooi and De Hosson, GeTe is inserted in the middle of Bi_2Te_3 quintuple layers as shown in Fig. 1(c) [35]. For higher compositions of Bi_2Te_3 ($m < n$), GBT compounds have mixed layers with one GeBi_2Te_4 and $(n - 1)\text{Bi}_2\text{Te}_3$ layers as shown in Fig. 1(b). In order to verify the tendency of the lattice parameters with various compositions of GeTe and Bi_2Te_3 , we have relaxed all the crystal structures and compared them to the experimental reports. The calculated lattice constants of GBT in Fig. 2(a) show good agreement with the experimental values within 2% error. This is coming from the choice of vdW interaction, where typical PBEs highly overestimate the lattice constants and vdW bond length [36–39]. The lattice constants a and c decrease linearly with the alloying ratio $(m + 2n)/(m + 3n)$. Figure 2(b) also shows the change of the

interlayer distances for each atomic species, which indicates little change of the interlayer distances for covalent Ge-Te and Bi-Te bonds, so the electronic structure of GBT compounds would be mainly affected by the change of lattice constant a . Note that there are clear differences in the Ge-Te interlayer distances between the GBT compounds and pure GeTe. In pure GeTe, the ferroelectricity makes the distortion in Ge-Te interlayer distances [40]. In the GBT compounds, however, the distortion in Ge-Te interlayer distances is much reduced and it becomes an almost cubiclike structure. Because cubic GeTe has been suggested as a thermoelectric material with a large value of ZT [41], the GBT can be considered a mixture of good TE materials, as will be discussed later.

We calculated the electronic structures, using relaxed crystal structures, and Fig. 3 shows the orbital projected density of states (DOS), band structures along the z direction (cross plane), and band-gap energy ($E_{e,g}$) of the GBT compounds. The $E_{e,g}$ for Bi_2Te_3 is 0.13 eV, comparable to experiment (~ 0.16 eV) [42]. The $E_{e,g}$ for GeTe is 0.34 eV, comparable to experiments (rhombohedral, 0.38–0.66 eV) [43–45]. For the GBT compounds, Ge and Bi p orbitals significantly contribute to the conduction-band edge of the band gap. The Te (1) at the center of the Bi_2Te_3 quintuple layer [Fig. 1(a)] contributes to the valence-band edge, while Te (2) in the vdW layers contributes to both conduction- and valence-band edges. The DOS and the band structures of GeBi_2Te_4 ($m = 1, n = 1$) in Fig. 3(b) are similar to those of Bi_2Te_3 in Fig. 3(a), as compared to those of GeTe in Fig. 3(c). The arrows and dashed

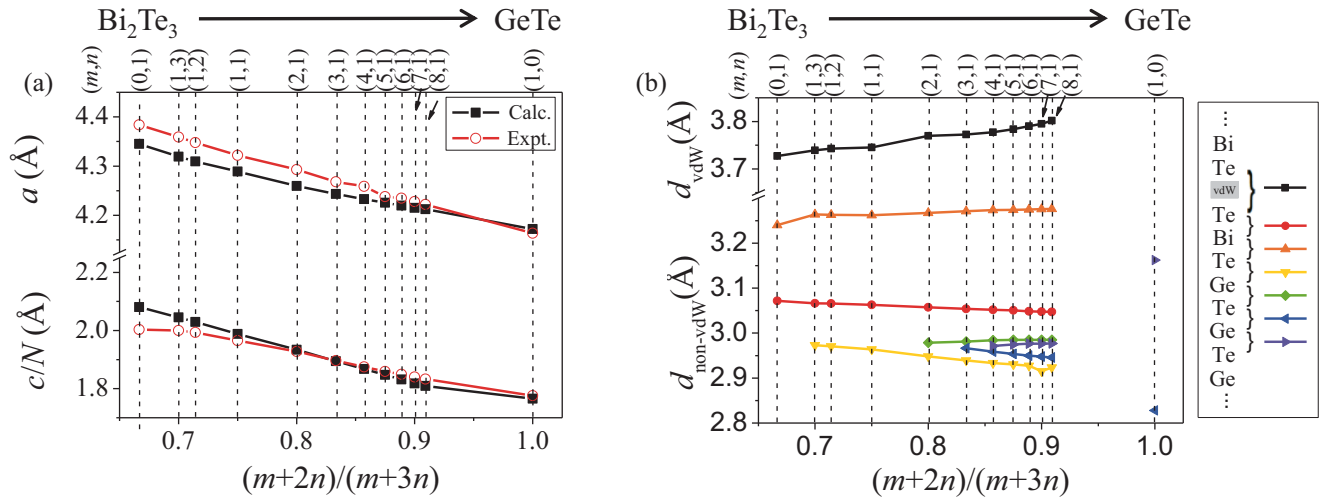


FIG. 2. (a) Lattice parameters a and c/N (N : number of atoms in unit cell) as a function of the alloying ratio $(m+2n)/(m+3n)$ which increases with high GeTe content [10,14]. The grid lines indicate the (m,n) compositions of GeTe and Bi₂Te₃. (b) Interlayer distances for each atomic layer. The GBT have $2m+5$ layers in the unit cell and m kind of interlayer distances. Each color describes interlayer distances from the vdW layers of gray color (Te-Te) to innermost atomic layers (Te-Ge or Ge-Te).

lines in Fig. 3 indicate band shifts. The bandwidth of Bi₂Te₃ (GeTe) enlarges (shrinks) with respect to their conduction and valence-band centers, due to the strain (tensile) in the in-plane lattice constant. Therefore, the bands with Bi₂Te₃ (GeTe) contribution shift toward (away from) the band-gap center. In Fig. S1 of the Supplemental Material, the DOS changes for the entire GBT compounds [46], becoming progressively

larger with higher GeTe content. In addition to shift in peaks, additional bands with Ge s -orbital contribution at the valence band (~ -0.3 eV) become dominant at high GeTe content. The combination of strain and appearance of the Ge s orbital causes asymmetry in DOS (heavier for valence band) at high GeTe content (Fig. S1). This results in an asymmetric Seebeck coefficient, with shift toward the conduction band.

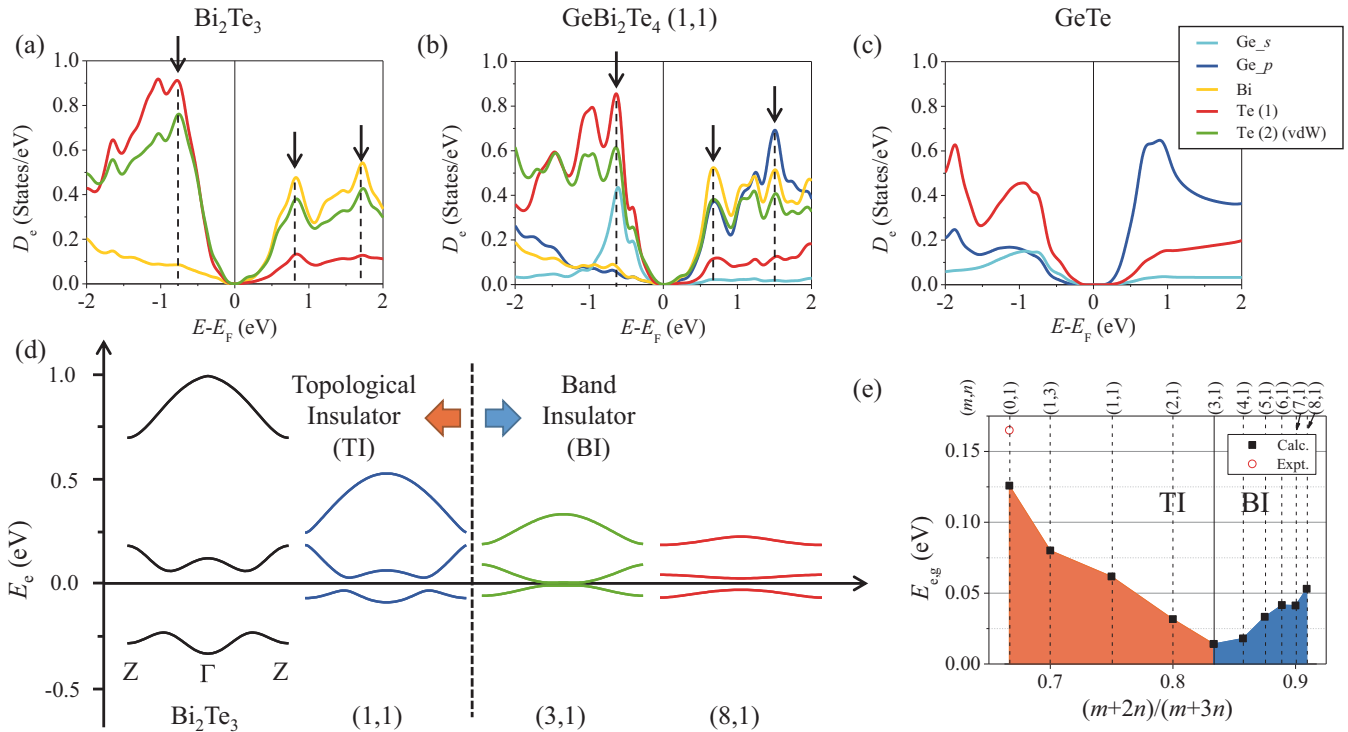


FIG. 3. (a-c) The DOS of Bi₂Te₃, GeBi₂Te₄ [(1, 1) composition], and GeTe with their orbital characteristics. The displacement of DOS peaks with similar orbital characteristics are indicated by arrows and dashed lines in the plot. (d) The variations in the band dispersion of Bi₂Te₃ and GBT along the z direction (cross plane) with composition. (e) Calculated band-gap energy of Bi₂Te₃ and the GBT compounds and comparison with experiments. Each color distinguishes the characteristics of the band gap as topological insulator and band insulator. See Fig. S1 for the variations of DOS and the band dispersion along the z direction of entire GBT compositions [46].

For moderate doping conditions where the chemical potential is located near the band gap, the Seebeck coefficient for the p -type GBT compounds increases, but for the n type it decreases (with sign change).

Another feature in the electronic structures of GBT compounds is the change of dimensionality due to the quantum-confinement effect on Bi_2Te_3 , where the insertion of the GeTe insulating layer separates the Bi_2Te_3 layers. The conduction-band minimum and valence-band maximum of GBT compounds have mainly Bi_2Te_3 characters near the Γ -Z symmetry line. Therefore the quantum-confinement effect reduces the band dispersion near the band gap with increasing GeTe ratio as shown in Fig. 3(d). According to the Mott formula [47], this flat-band dispersion results in high Seebeck coefficient along the out-of-plane direction for high GeTe content as will be discussed in Sec. III C. With the combination of the strain effect and the quantum-confinement effect, the obtained $E_{e,g}$'s of whole GBT compounds are lower than that of Bi_2Te_3 , as summarized in Fig 3(e). The GST compounds with the rhombohedral phase are reported to have almost zero band gap [48], which is also consistent with our results. It is interesting that Bi_2Te_3 , GeBi_2Te_4 ($m = 1, n = 1$), and $\text{Ge}_2\text{Bi}_2\text{Te}_5$ ($m = 2, n = 1$) behave as topological insulators because of the band-gap inversion induced by the strong SO interaction in Bi atoms [24–27]. As the band dispersion becomes flatter, however, the band-gap inversion disappears beyond $\text{Ge}_3\text{Bi}_2\text{Te}_6$ ($m = 3, n = 1$), which results in minimum $E_{e,g}$, and GBT compounds with higher GeTe content become normal insulators.

B. Semiempirical approach of electron scattering time

For the calculation of electrical conductivity within the usual BTE calculation, a constant scattering time approximation (CSTA) is used because the exact description of τ_e is challenging due to its multiple mechanisms [30]. The Seebeck coefficients for various TE materials are well reproduced using the BTE with the CSTA [30,49–53], since the constant τ_e cancels out in the calculation steps. However, the electrical conductivity in the BTE only considers the group velocities of the electrons (effective mass) and their thermal activation (carrier concentration) from the bands' structures. Figure S2 [46] shows the electrical conductivity tensor ($\Sigma_{e,\text{BTE}}$) from the BTE with the CSTA, for several GBT compounds and Bi_2Te_3 . Compared to the experimental electrical conductivity in Figs. S3(a) and S3(b) [46], there is weak temperature dependence. The complex scattering mechanisms such as electron-phonon scattering, electron-impurity scattering, and point-defect scattering result in temperature dependence of the electrical conductivity, and cannot be realistically included in the CSTA. Therefore, an accurate description of the temperature- and doping-dependent τ_e is critical in predicting the electrical conductivity [54,55]. There have been many attempts to determine each scattering parameter from the first-principles calculations within density perturbation functional theory (DFPT) [56] or by the empirical Kane model considering nonparabolic band dispersion fitted by experimental data [57,58]. However, the DFPT calculations cannot consider the entire scattering mechanisms and the Kane model requires many complicated fitting parameters.

We employed a semiempirical approach to describe τ_e from the electrical conductivity tensor from the BTE [$\Sigma_{e,\text{BTE}}(T, \mu)$] and the experimental conductivity [$\sigma_{e,\text{exp}}(T)$] [12,59–64].

$$\tau_e(T, \mu) = \sigma_{e,\text{exp}}(T, \mu) / \Sigma_{e,\text{BTE}}(T, \mu), \quad (1)$$

where $\Sigma_{e,\text{BTE}}(T, \mu)$ is the directional average of the electrical conductivity tensor $\Sigma_{e,\alpha\beta}(T, \mu)$, given by

$$\Sigma_{e,\alpha\beta}(T, \mu) = \frac{1}{V} \int \Sigma_{e,\alpha\beta}(\varepsilon) \left\{ -\frac{\partial f_\mu(T; \varepsilon)}{\partial \varepsilon} \right\} d\varepsilon, \quad (2)$$

$$\Sigma_{e,\alpha\beta}(\varepsilon) \equiv \sigma_{e,\alpha\beta}(\varepsilon) / \tau_e = \frac{1}{N} \sum_{i,\mathbf{k}} e^2 v_\alpha(i, \mathbf{k}) v_\beta(i, \mathbf{k}) \delta(\varepsilon - \varepsilon_{i,\mathbf{k}}), \quad (3)$$

where i describes the band index, \mathbf{k} describes the momentum in the Brillouin zone, and the greek letters (α, β) describe the directional index. V is the volume of the unit cell, N is the number of \mathbf{k} points sampled, $v_\alpha(i, \mathbf{k})$ is the group velocity of the electron ($=1/\hbar \cdot \nabla_{\mathbf{k}} \varepsilon_{i,\mathbf{k}}$), and $f_\mu(T; \varepsilon)$ is the Fermi-Dirac distribution at temperature T with chemical potential μ . Here, we assume constant τ_e for given momentum and band index, but consider its variation with T and μ . Then we estimate $\tau_e(T, \mu)$ with experimental conductivities and the conductivity tensor from the first-principles calculations, for various compounds.

The predicted $\tau_e(T, \mu)$ is compared with experimental results for Bi_2Te_3 and GBT compounds, and summarized in Fig. S3 [46]. For Bi_2Te_3 of moderate carrier density ($\sim 10^{19} \text{ cm}^{-3}$), τ_e^{-1} are similar and consistent with the empirical Kane model [58]. The averaged τ_e^{-1} for Bi_2Te_3 shown in Fig. S3(e) is consistent with experiments [59–64], and follows $\sim T^{2.5}$ representing the two-phonon processes in electron-acoustic phonon scattering of nondegenerate semiconductors [54,65]. For the GBT compounds of high carrier density ($> 2 \times 10^{20} \text{ cm}^{-3}$), τ_e^{-1} has a behavior expected from the measured conductivity. Here, we use $\tau_e^{-1} = \tau_r^{-1} + AT$, where τ_r^{-1} represents the residual scattering rate and T is based on the electron-acoustic phonon scattering for highly degenerate semiconductors. The scatter in τ_r^{-1} arises from the sample quality (impurity, defect, etc.). So, we choose τ_r^{-1} to give consistent electrical conductivity at room temperature for the GBT compounds [15]. We expect the scattering rate to be nearly the same for the GBT compounds and Bi_2Te_3 , for a given carrier density, due to the similar crystal and the band structures. We use the electron scattering time of the Bi_2Te_3 at 10^{19} cm^{-3} (Fig. 4) for the entire GBT compounds at the same doping, and the scattering time of the GBT compounds at $4 \times 10^{20} \text{ cm}^{-3}$ for Bi_2Te_3 at the same doping (Fig. 5).

C. TE properties

GBT compounds have naturally high carrier concentration in nature due to the nonstoichiometry of both GeTe and Bi_2Te_3 parts. GeTe is usually highly doped p -type material ($p > 2 \times 10^{20} \text{ cm}^{-3}$) with excess Te [66], while Bi_2Te_3 is n type with excess Bi [67]. Therefore the GBT compounds become p type for high GeTe content ($m > n$) and n type for high Bi_2Te_3 content ($m < n$) [10]. Based on the DFT band structures, we have calculated the temperature-dependent TE properties (electrical conductivity, Seebeck coefficient,

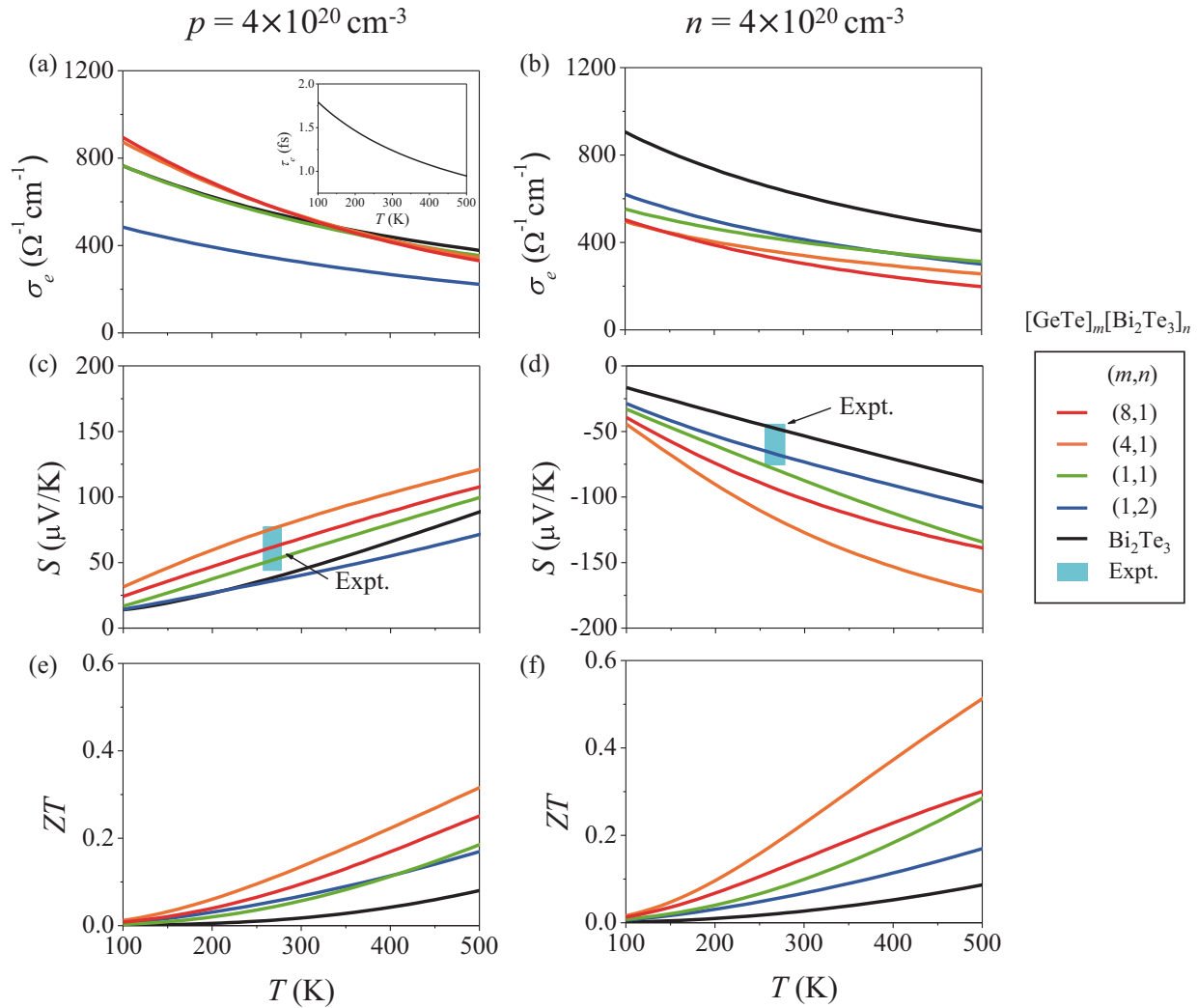


FIG. 4. The calculated temperature-dependent (a,b) electrical conductivities; (c,d) Seebeck coefficient; and (e,f) ZT of the GBT compounds at doping $p(n) = 4 \times 10^{20} \text{ cm}^{-3}$, compared to those of Bi_2Te_3 . Inset: The calculated τ_e from Eq. (1) [46].

and ZT) of compounds at both hole and electron doping of 10^{19} cm^{-3} and $4 \times 10^{20} \text{ cm}^{-3}$, using the BTE with the semiempirical description of the scattering time as described above. Note that we only compare the TE properties of Bi_2Te_3 and GBT compounds because the GeTe has a different crystal structure from that of the GeTe in GBT (which results in different electronic structure, as we discussed [41,68]).

Based on the calculated τ_e [inset in Figs. 4(a) and 5(a)], the experimental electrical conductivities (Figs. 4 and 5) are well reproduced at both moderate (10^{19} cm^{-3}) [61,63,64] and high carrier concentration ($4 \times 10^{20} \text{ cm}^{-3}$) [13,14,69]. Note that all the GBT compounds are well described with the same scattering rate, which indicates that the scattering mechanism should be similar between each compound at a given carrier concentration. Since we have assumed the same carrier concentration and residual scattering time τ_r for all compounds, the small disagreement with experimental data can be acceptable. At high carrier concentrations shown in Figs. 4(a) and 4(b), the electrical conductivities show almost similar results for all GBT compounds and Bi_2Te_3 , since they have similar electronic structures at high chemical potential, while the n -type Bi_2Te_3 has higher conductivity due to larger

group velocity with more dispersive conduction bands as shown in Fig. 3(d). At moderate carrier concentration shown in Figs. 5(a) and 5(b), the electrical conductivities of GBT compounds generally show lower values than those of Bi_2Te_3 , due to their flatter band structures near the band gap [Fig. 3(d)]. For the case of p -type GBT, the increased contribution of the Ge s orbital at high GeTe content results in high conductivity close to that of Bi_2Te_3 . For the n -type cases, there are no such states and the electrical conductivities decrease monotonically as the GeTe content increases.

For the Seebeck coefficient, our results are consistent with experiments from GBT compounds, presented in Figs. 4 and 5, at room temperature. Here, the n -type GBT compounds show larger Seebeck coefficient compared to experiments, understandable since the experiments are restricted to large Bi_2Te_3 contents. In Fig. S4 [46], the temperature dependence is also well predicted by our BTE treatment. At high carrier densities, the chemical potential is high enough (± 0.3 – 0.5 eV) and the Seebeck coefficient is affected by the DOS peak. The Seebeck coefficient of GBT compounds is higher compared to Bi_2Te_3 , due to more pronounced DOS peak shifted toward the band gap. Compared to the p -type compounds, the n type

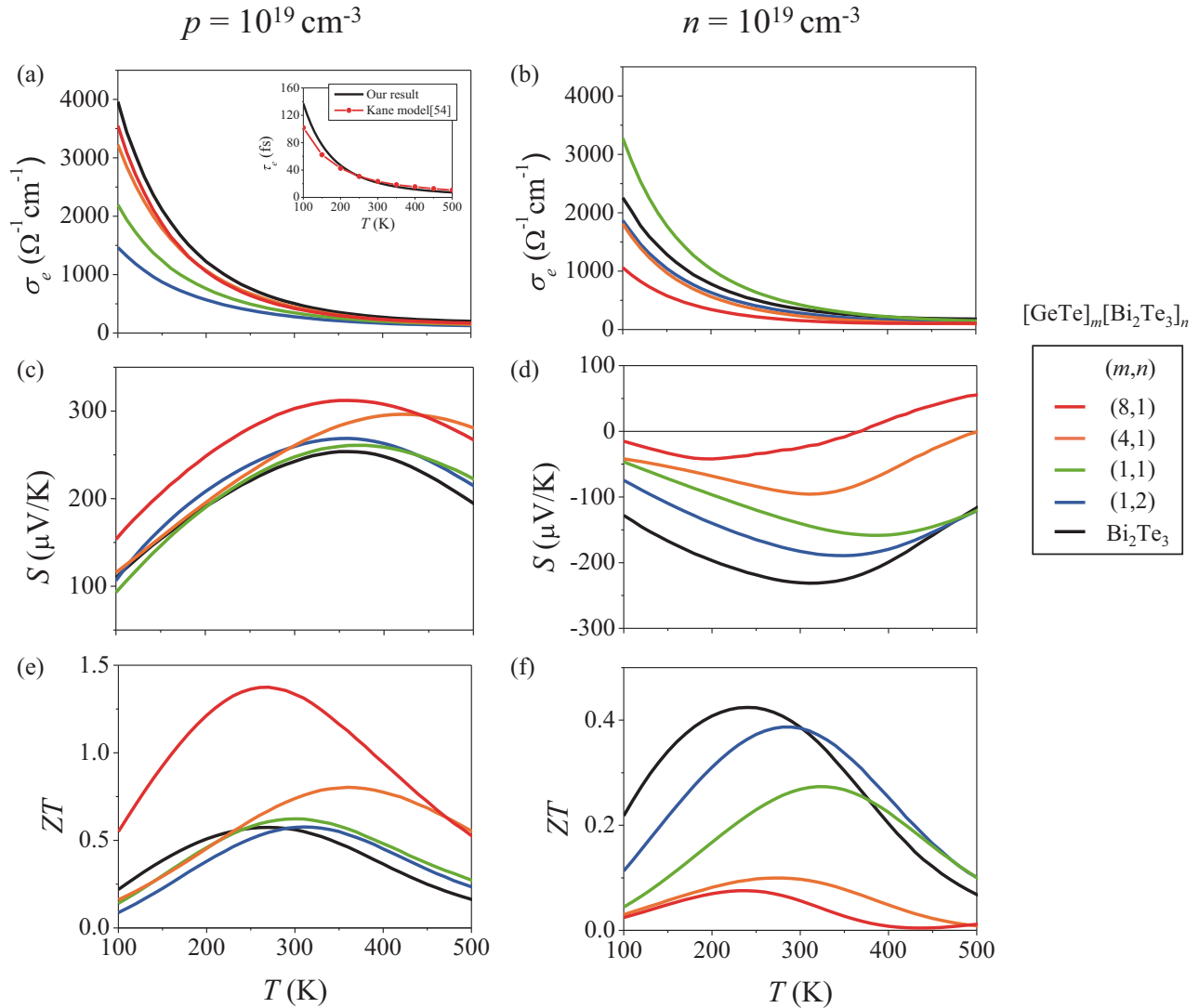


FIG. 5. The calculated temperature-dependent (a,b) electrical conductivities; (c,d) Seebeck coefficient; and (e,f) ZT the GBT compounds at moderate carrier concentration $p(n) = 10^{19} \text{ cm}^{-3}$, compared to those of Bi_2Te_3 . Inset: The calculated τ_e from Eq. (1) [46]. It is compared to other reports with the Kane model [58].

shows larger Seebeck coefficient (larger and sharper DOS peak at conduction band). For moderate carrier concentration, the strain and the quantum-confinement effects (Sec. III A), result in asymmetry and large Seebeck coefficient of the p -type GBT compounds at high GeTe contents. However, the n -type GBT compounds have smaller Seebeck coefficient (and sign change with temperature).

To calculate ZT , we have used the constant lattice thermal conductivities (κ_l) whose values are comparable to the experimental values near 300 K: 1.2 W/m K for Bi_2Te_3 [63] and 0.5 W/m K for whole GBT compounds [14]. Also, the electrical thermal conductivity is calculated using the Wiedemann-Franz law [70]. At high carrier concentration shown in Fig. 4, small electrical conductivity and Seebeck coefficients result in small ZT of GBT compounds. Despite the small band gap, whole compounds show the enhancement of ZT with increasing temperature, which is the characteristic of a highly degenerated semiconductor. At moderate carrier concentration shown in Fig. 5, the p -type GBT compounds show better

TE performances than Bi_2Te_3 with a combination of larger Seebeck coefficient and lower lattice thermal conductivity, while retaining comparable electrical conductivity. Among the considered compounds, $\text{Ge}_8\text{Bi}_2\text{Te}_{11}$ ($m = 8, n = 1$) is predicted to have the best TE performances with $ZT = 1.4$.

To check the validity of our results, we have compared our calculated ZT with experimental reports, as summarized in Fig. 6. Here, we have chosen experimental results for the optimal ZT at moderate carrier concentration and room temperature ZT values at high carrier concentration. To show the possible ZT ranges near room temperature, we have plotted the calculated ZT at various temperature ranges (200–400 K). For moderate carrier concentration, there are few experimental results supporting our calculations, but all show good agreement. Our results show that the band engineering by lattice-strain and quantum-confinement effect on GBT compounds can enhance the ZT of the p -type Bi_2Te_3 up to 1.4. We expect changing Bi_2Te_3 to $(\text{Bi}_{1-x}\text{Sb}_x)_2\text{Te}_3$, which has higher ZT (~ 1.5) [71], can further enhance the ZT . Note

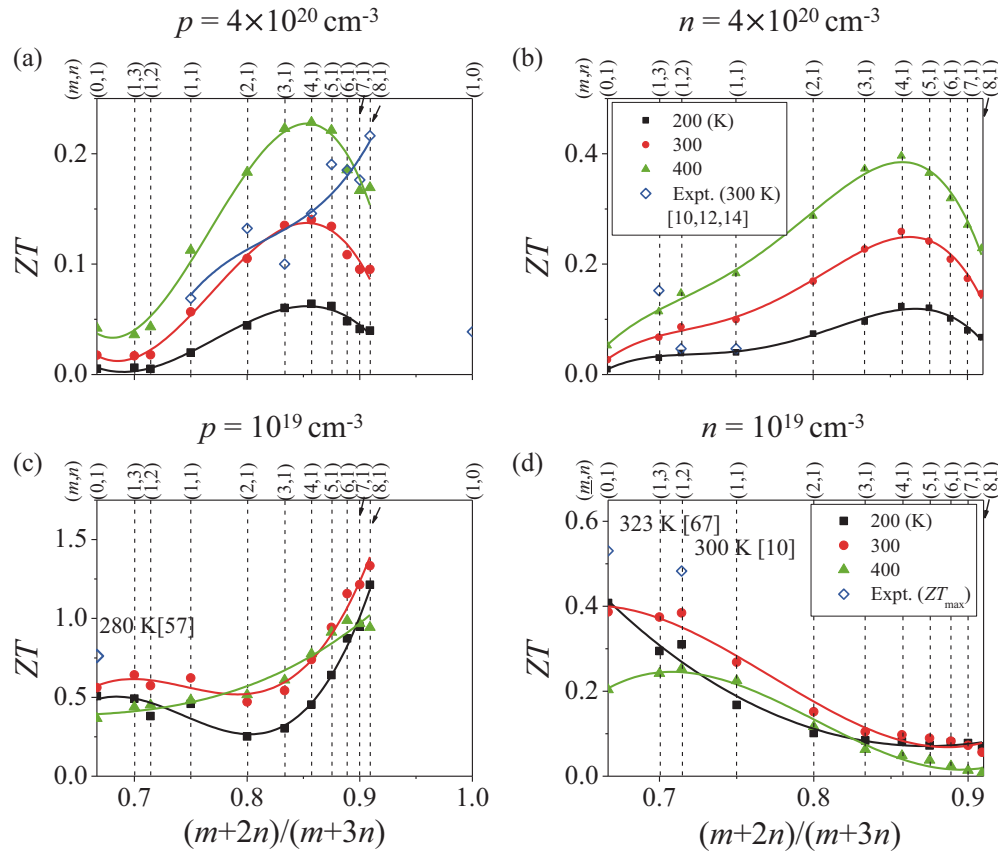


FIG. 6. Comparison of calculated ZT with experiments for Bi₂Te₃ [61,73] and the GBT compounds [10,12,14] as a function of composition $(m + 2n)/(m + 3n)$. For high carrier concentration $p(n) = 4 \times 10^{20} \text{ cm}^{-3}$ (a,b), we have chosen experimental ZT at room temperature. For moderate carrier concentration $p(n) = 10^{19} \text{ cm}^{-3}$ (c,d), we have chosen experimental data of optimal ZT for each plot.

that this carrier density regime may not be optimal for the best thermoelectric performance because the data on scattering properties as function of temperature are available only for two conditions (10^{19} and $4 \times 10^{20} \text{ cm}^{-3}$) given by Fig. S3 [46]. At high doping, the calculated ZT shows good agreement with experimental results. The discrepancy in variation of ZT with composition can be due to the residual resistivity of the GBT compounds. All GBT show enhanced ZT at room temperature, compared to pure GeTe. The obtained ZT is similar to that of the cubic Ge_{1-x}Pb_xTe with Bi₂Te₃ doping, which shows high ZT (~ 1.9) at 800 K [21]. Although the electronic structures of GBT compounds and GeTe are much different, it shows that high-dopant GBT compounds could be used in TE devices in the intermediate temperature range.

IV. CONCLUSIONS

In summary, we have checked the electronic structure and TE properties of GBT compounds for various compositions ($1 \leq m \leq 8, 1 \leq n \leq 3$). GBT compounds are the mixture of GeTe and Bi₂Te₃, where GeTe intercalated into Bi₂Te₃ quintuple layers. The band structures of GBT compounds are similar to that of Bi₂Te₃ with in-plane strain effect. Also, the separation of Bi₂Te₃ quintuple layers with a large-band-gap semiconductor GeTe makes for significant quantum-confinement effect on the electronic structures of Bi₂Te₃. With the combination of these two effects, the electronic structures

of the GBT compounds have asymmetric distribution of DOS and flat-band dispersion near the band gap. On the basis of the electronic structures, we have explored the temperature-dependent TE performance, using semiempirical electron scattering time. Our results show good agreement with the reported experimental results for high carrier concentration ($4 \times 10^{20} \text{ cm}^{-3}$) [13,14]. It shows enhancement of ZT over the pure GeTe, considered as good TE material in the intermediate-temperature range [21]. For moderate carrier concentration (10^{19} cm^{-3}), which is optimal doping for Bi₂Te₃ [59–64], the *p*-type GBT with $m = 8, n = 1$ is predicted to have best ZT up to 1.4 near room temperature. The results show that band engineering by strain and quantum-confinement effect could enhance the TE performances. Also, our semiempirical τ_e can be used to guide search optimal composition for other TE systems.

ACKNOWLEDGMENTS

We thank Prof. Jeunghye Park for useful discussion. This research was supported by Global Frontier Program through the Global Frontier Hybrid Interface Materials (GFHIM) of the National Research Foundation of Korea (NRFK) funded by the Ministry of Science, ICT & Future Planning (Grant No. 2013M3A6B1078870). M.K. is grateful for support from the US National Science Foundation program on Thermal Transport and Processes (Award No. CBET1332807).

- [1] I. Terasaki, Y. Sasago, and K. Uchinokura, *Phys. Rev. B*, **56**, R12685 (1997).
- [2] M. G. Kanatzidis, *Acc. Chem. Res.* **38**, 359 (2004).
- [3] O. G. Karpinskii, L. E. Shelimova, M. A. Kretova, E. S. Avilov, and V. S. Zemskov, *Inorg. Mater.* **39**, 240 (2003).
- [4] L. E. Shelimova, O. G. Karpinskii, T. E. Svechnikova, E. S. Avilov, M. A. Kretova, and V. S. Zemskov, *Inorg. Mater.* **40**, 1264 (2004).
- [5] N. Chen, F. Gascoin, G. J. Snyder, E. Müller, G. Karpinski, and C. Stiewe, *Appl. Phys. Lett.* **87**, 171903 (2005).
- [6] B. A. Cook, M. J. Kramer, X. Wei, J. L. Harringa, and E. M. Levin, *J. Appl. Phys.* **101**, 053715 (2007).
- [7] L. D. Zhao, D. Berardan, Y. L. Pei, C. Byl, L. Pinsard-Gaudart, and N. Dragoe, *Appl. Phys. Lett.* **97**, 092118 (2010).
- [8] S. P. Li, J. Q. Li, Q. B. Wang, L. Wang, F. S. Liu, and W. Q. Ao, *Solid State Sci.* **13**, 399 (2011).
- [9] C. Lee, J. Hong, M.-H. Whangbo, and J. H. Shim, *Chem. Mater.* **25**, 3745 (2013).
- [10] L. E. Shelimova, O. G. Karpinsky, M. A. Kretova, E. S. Avilov, and J. P. Fleurial, in *Proceedings of the XVI International Conference on Thermoelectrics, 1997* (IEEE, New York, 1997), p. 481.
- [11] O. G. Karpinsky, L. E. Shelimova, M. A. Kretova, and J. P. Fleurial, *J. Alloys Compd.* **265**, 170 (1998).
- [12] P. P. Konstantinov, L. E. Shelimova, E. S. Avilov, M. A. Kretova, and J. P. Fleurial, *J. Solid State Chem.* **146**, 305 (1999).
- [13] L. E. Shelimova, P. P. Konstantinov, O. G. Karpinsky, E. S. Avilov, M. A. Kretova, and J. P. Fleurial, in *Proceedings of the XVIII International Conference on Thermoelectrics, 1999* (IEEE, New York, 1999), p. 536.
- [14] L. E. Shelimova, P. P. Konstantinov, O. G. Karpinsky, E. S. Avilov, M. A. Kretova, and V. S. Zemskov, *J. Alloys Compd.* **329**, 50 (2001).
- [15] L. E. Shelimova, O. G. Karpinskii, P. P. Konstantinov, E. S. Avilov, M. A. Kretova, and V. S. Zemskov, *Inorg. Mater.* **40**, 451 (2004).
- [16] N. Yamada, E. Ohno, K. Nishiuchi, N. Akahira, and M. Takao, *J. Appl. Phys.* **69**, 2849 (1991).
- [17] C. W. Sun, M. S. Youm, and Y. T. Kim, *J. Phys.: Condens. Matter* **19**, 446004 (2007).
- [18] M. Wuttig and N. Yamada, *Nat. Mater.* **6**, 824 (2007).
- [19] L. E. Shelimova, O. G. Karpinskii, P. P. Konstantinov, M. A. Kretova, E. S. Avilov, and V. S. Zemskov, *Inorg. Mater.* **38**, 790 (2002).
- [20] L. Weintraub, J. Davidow, J. Tunbridge, R. Dixon, M. J. Reece, H. Ning, I. Agote, and Y. Gelbstein, *J. Nanomater.* **2014**, 284634 (2014).
- [21] D. Wu, L.-D. Zhao, S. Hao, Q. Jiang, F. Zheng, J. W. Doak, H. Wu, H. Chi, Y. Gelbstein, C. Uher, C. Wolverton, M. Kanatzidis, and J. He, *J. Am. Chem. Soc.* **136**, 11412 (2014).
- [22] C. S. Jung, H. S. Kim, H. S. Im, K. Park, J. Park, J. P. Ahn, S. J. Yoo, J. G. Kim, J. N. Kim, and J. H. Shim, *Nano Lett.* **15**, 3923 (2015).
- [23] L. Zhang and D. J. Singh, *Phys. Rev. B*, **81**, 245119 (2010).
- [24] T. V. Menshchikova, S. V. Ereemeev, Y. M. Koroteev, V. M. Kuznetsov, and E. V. Chulkov, *JETP Lett.* **93**, 15 (2011).
- [25] J. Kim, J. Kim, K.-S. Kim, and S.-H. Jhi, *Phys. Rev. Lett.* **109**, 146601 (2012).
- [26] M. Neupane, S. Y. Xu, L. A. Wray, A. Petersen, R. Shankar, N. Alidoust, C. Liu, A. Fedorov, H. Ji, J. M. Allred, Y. S. Hor, T. R. Chang, H. T. Jeng, H. Lin, A. Bansil, R. J. Cava, and M. Z. Hasan, *Phys. Rev. B*, **85**, 235406 (2012).
- [27] S. V. Ereemeev, G. Landolt, T. V. Menshchikova, B. Slomski, Y. M. Koroteev, Z. S. Aliev, M. B. Babanly, J. Henk, A. Ernst, L. Patthey, A. Eich, A. A. Khajetoorians, J. Hagemeyer, O. Pietzsch, J. Wiebe, R. Wiesendanger, P. M. Echenique, S. S. Tsirkin, I. R. Amiraslanov, J. H. Dil, and E. V. Chulkov, *Nat. Commun.* **3**, 635 (2012).
- [28] G. Kresse and J. Furthmüller, *Phys. Rev. B*, **54**, 11169 (1996).
- [29] P. Blaha, K. Schwarz, G. Madsen, D. Kvasnicka, and J. Luitz, *WIEN2K, An Augmented Plane Wave+Local Orbitals Program for Calculating Crystal Properties*, 2001.
- [30] G. K. H. Madsen and D. J. Singh, *Comput. Phys. Commun.* **175**, 67 (2006).
- [31] J. P. Perdew, K. Burke, and M. Ernzerhof, *Phys. Rev. Lett.* **77**, 3865 (1996).
- [32] S. Grimme, *J. Comput. Chem.* **27**, 1787 (2006).
- [33] A. T. Clay, C. M. Kuntz, K. E. Johnson, and A. L. L. East, *J. Chem. Phys.* **136** (2012).
- [34] E. Engel and S. H. Vosko, *Phys. Rev. B*, **47**, 13164 (1993).
- [35] B. J. Kooi and J. T. M. De Hosson, *J. Appl. Phys.* **92**, 3584 (2002).
- [36] X. Luo, M. B. Sullivan, and S. Y. Quek, *Phys. Rev. B*, **86**, 184111 (2012).
- [37] V. L. Deringer and R. Dronskowski, *J. Phys. Chem. C* **117**, 15075 (2013).
- [38] L. Cheng, H. J. Liu, J. Zhang, J. Wei, J. H. Liang, J. Shi, and X. F. Tang, *Phys. Rev. B*, **90**, 085118 (2014).
- [39] B.-T. Wang, P. Souvatzis, O. Eriksson, and P. Zhang, *J. Chem. Phys.* **142**, 174702 (2015).
- [40] A. I. Lebedev, I. A. Sluchinskaya, V. N. Demin, and I. H. Munro, *Phase Transitions* **60**, 67 (1997).
- [41] X. Chen, D. Parker, and D. J. Singh, *Sci. Rep.* **3**, 3168 (2013).
- [42] R. Sehr and L. R. Testardi, *J. Phys. Chem. Solids* **23**, 1219 (1962).
- [43] S. Yamanaka, S. Ogawa, I. Morimoto, and Y. Ueshima, *Jpn. J. Appl. Phys.* **37**, 3327 (1998).
- [44] J.-W. Park, S. H. Eom, H. Lee, J. L. F. Da Silva, Y.-S. Kang, T.-Y. Lee, and Y. H. Khang, *Phys. Rev. B*, **80**, 115209 (2009).
- [45] D. J. Singh, *J. Appl. Phys.* **113**, 203101 (2013).
- [46] See Supplemental Material at <http://link.aps.org/supplemental/10.1103/PhysRevB.93.075119> for the change of DOS with varying GeTe and Bi₂Te₃ compositions, the electrical conductivity tensor from the BTE with the CSTA, the information for τ_e , and the comparison between the calculated Seebeck coefficients and the experimental one.
- [47] M. S. Dresselhaus, G. Chen, M. Y. Tang, R. G. Yang, H. Lee, D. Z. Wang, Z. F. Ren, J. P. Fleurial, and P. Gogna, *Adv. Mater.* **19**, 1043 (2007).
- [48] D. Subramaniam, C. Pauly, M. Liebmann, M. Woda, P. Rausch, P. Merkelbach, M. Wuttig, and M. Morgenstern, *Appl. Phys. Lett.* **95** (2009).
- [49] G. K. H. Madsen, *J. Am. Chem. Soc.* **128**, 12140 (2006).
- [50] J.-S. Rhyee, K. H. Lee, S. M. Lee, E. Cho, S. I. Kim, E. Lee, Y. S. Kwon, J. H. Shim, and G. Kotliar, *Nature* **459**, 965 (2009).
- [51] C. Sevik and T. Çağın, *Appl. Phys. Lett.* **95**, 112105 (2009).
- [52] D. J. Singh, *Phys. Rev. B* **81**, 195217 (2010).

- [53] J. M. Tomczak, K. Haule, and G. Kotliar, *Proc. Natl. Acad. Sci. USA* **109**, 3243 (2012).
- [54] B. M. Askerov, *Electron Transport Phenomena in Semiconductors* (World Scientific, Singapore, 1994).
- [55] N. W. Ashcroft and N. D. Mermin, *Solid State Physics* (Holt, Rinehart and Winston, New York, 1976).
- [56] J. Sjakste, N. Vast, and V. Tyuterev, *Phys. Rev. Lett.* **99**, 236405 (2007).
- [57] E. O. Kane, *J. Phys. Chem. Solids* **1**, 249 (1957).
- [58] B.-L. Huang and M. Kaviani, *Phys. Rev. B* **77**, 125209 (2008).
- [59] H. J. Goldsmid, *Proc. Phys. Soc., London, Sec. B* **69**, 203 (1956).
- [60] S. Shigetomi and S. Mori, *J. Phys. Soc. Jpn.* **11**, 915 (1956).
- [61] H.-W. Jeon, H.-P. Ha, D.-B. Hyun, and J.-D. Shim, *J. Phys. Chem. Solids* **52**, 579 (1991).
- [62] L. Jansa, P. Lošťák, J. Šrámková, and J. Horák, *J. Mater. Sci.* **27**, 6062 (1992).
- [63] L. D. Ivanova and Y. V. Granatkina, *Inorg. Mater.* **36**, 672 (2000).
- [64] V. A. Kulbachinskii, V. G. Kytin, A. A. Kudryashov, and P. M. Tarasov, *J. Solid State Chem.* **193**, 47 (2012).
- [65] E. Z. Gershtein, T. S. Stavitskaya, and L. S. Stil'bans, *Sov. Phys. Tech. Phys.* **2**, 2302 (1957).
- [66] K. L. Chopra and S. K. Bahl, *J. Appl. Phys.* **40**, 4171 (1969).
- [67] C. B. Satterthwaite and R. W. Ure, Jr., *Phys. Rev.* **108**, 1164 (1957).
- [68] L. Xu, H.-Q. Wang, and J.-C. Zheng, *J. Electron. Mater.* **40**, 641 (2011).
- [69] S. Bäbler, T. Böhnert, J. Gooth, C. Schumacher, E. Pippel, and K. Nielsch, *Nanotechnology* **24**, 495402 (2013).
- [70] R. Franz and G. Wiedemann, *Ann. Phys. Chem.* **165**, 497 (1853).
- [71] W. Xie, X. Tang, Y. Yan, Q. Zhang, and T. M. Tritt, *Appl. Phys. Lett.* **94**, 102111 (2009).
- [72] K. Momma and F. Izumi, *J. Appl. Crystallogr.* **44**, 1272 (2011).
- [73] L.-D. Zhao, B.-P. Zhang, W.-S. Liu, and J.-F. Li, *J. Appl. Phys.* **105**, 023704 (2009).